53rd AIAA/ASME/ASCE/AHS/ASC Structures, Structural Dynamics and Materials Conference
20th AI
23 - 26 April 2012, Honolulu, Hawaii

AIAA 2012-1563

Lyapunov Inverse Iteration for Stability Analysis using Computational Fluid Dynamics

S. Timme* and K. J. Badcock†

University of Liverpool, Liverpool, England L63 3GH, United Kingdom

M. Wu‡

University of Maryland, College Park, MD 20742, United States

A. Spence§

University of Bath, Bath, England BA2 7AY, United Kingdom

The recently developed inexact Lyapunov inverse iteration method is presented for the analysis of aeroelastic and fluid stability problems with Hopf bifurcations when using computational fluid dynamics in the modelling. The idea is to take the Jacobian matrix and its derivative with respect to an independent parameter, both evaluated at an equilibrium point, to obtain estimates of the critical eigenpair in addition to the critical value of the independent parameter. Prior knowledge of a frequency estimate, required as shift in standard inverse iteration, is not needed. The test cases presented include a two–degrees–of–freedom aerofoil and a flexible wing encountering flutter, and unsteady vortex shedding behind a circular cylinder in low Reynolds number flow.

Nomenclature

A	Jacobian matrix
B	Derivative of Jacobian matrix with respect to α
$\boldsymbol{f}$	Residual vector
M	Mass matrix
n	Dimension of problem
$R, \mathfrak{R}$	Residuals of Lyapunov equation and matrix eigenvalue problem, respectively
$\boldsymbol{r}$	Residual of eigenvalue problem, $\boldsymbol{r} = (A + \lambda B)\boldsymbol{x} - \mu M \boldsymbol{x}$
$\boldsymbol{w}$	Vector of unknowns
$\boldsymbol{x}, \boldsymbol{z}$	Eigenvector
Z	Eigenvector, $vec(Z) = \boldsymbol{z}$
α	Independent parameter (e.g. Reynolds number, altitude, etc.)
δ	Constant for inexact iterations
λ	Eigenvalue of problem with Kronecker structure, $\lambda = \alpha - \alpha_0$
μ	Eigenvalue, $\mu = \gamma \pm i\omega$
σ	Shift

Subscript

c	Critical condition (i.e. Hopf point)
f	Fluid
s	Structure
0	Equilibrium

*Research Associate, School of Engineering; sebastian.timme@liverpool.ac.uk.
†Professor, School of Engineering; k.j.badcock@liverpool.ac.uk.
‡PhD Student, Department of Mathematics; mwu@math.umd.edu.
§Professor, School of Mathematical Sciences; a.spence@maths.bath.ac.uk.

I. Introduction

The full range of fluid/structure interaction, including phenomena such as violent flutter, limit cycle oscillation and buffeting, requires computational fluid dynamics (CFD) methods for modelling the unsteady aerodynamics accurately. Approaches using linear aerodynamics can fail in certain situations as the underlying dominant physics of the fluid flow, including shock waves, shock boundary layer interaction and separation, are not accounted for. The limitations are well known (while the computational cost remains the paramount argument in favour of linear aerodynamics) and corrections are applied to extend the analysis to the important transonic flight regime. In this work, we are interested in the modelling of the aeroelastic system using nonlinear aerodynamics based on CFD methods, and methods to make the use of these high fidelity tools tractable are the main concern.

Advances in algorithms and computing power over the last decades have made CFD aerodynamic modelling feasible for the analysis of full aircraft configurations. However, in the aeroelastic context, reduced order modelling in various forms is an active area of investigation as the large number of analyses required for a single aircraft, including all possible load conditions and aircraft/store configurations, is the limiting factor. An alternative viewpoint to model reduction is the development of more efficient tools working with the full aerodynamic system instead. Rather than solving the full unsteady nonlinear problem, the fluid dynamics equations are often linearised by introducing small perturbations leading to the frequency domain. More specifically, nonlinear flow features such as transonic shocks and boundary layer separation are contained in the underlying steady flow solution, while dynamic perturbations about this nonlinear static equilibrium are linear. This approach is powerful for calculating the onset of an instability. Savings in computational cost of an order of magnitude are commonly stated.[1] The downside of dynamically linear modelling is a possible interest in the (large) amplitude of a limit cycle beyond the onset. However, it has been demonstrated that, in the vicinity of instability onset, a nonlinear model reduction based on the critical eigenspace can predict the growth of aeroelastic limit cycle amplitude.[2,3]

In this paper we are looking at the stability of nonlinear dynamical systems arising from fluid–only and fluid/structure coupled problems, using CFD aerodynamics and modal structural representations, which can be written in semidiscrete form as

$$M\frac{d\boldsymbol{w}}{dt} = \boldsymbol{f}\big(\boldsymbol{w}(\alpha), \alpha\big) \tag{1}$$

where the vectors $\boldsymbol{w}$ and $\boldsymbol{f}$ contain the unknowns and corresponding residuals, respectively, while α is a physical parameter to be specified. The stability of an equilibrium $\boldsymbol{w}_0(\alpha)$ (i.e. a steady state solution) of the dynamical system with respect to changes in α is sought, which results in an eigenvalue problem of the general form

$$A\boldsymbol{x} = \mu M\boldsymbol{x} \tag{2}$$

where in our case numerical discretisation of the physical problem results in M being the identity matrix, and $\boldsymbol{x}$ is the complex amplitude of the perturbation $\delta\boldsymbol{w} = \boldsymbol{x}e^{\mu t}$ with $\mu = \gamma \pm i\omega$ as an eigenvalue. Hidden in the latter notation is the dependence on the parameter α. Stability requires all eigenvalues to have a negative real part, and a change in stability arises when the rightmost eigenvalue crosses the imaginary axis of the complex plane for a critical value of α. We are interested in the case when stability of the system is lost through a Hopf bifurcation (i.e. a pair of complex conjugate eigenvalues with zero real part) consequently leading to periodic oscillations.

In early work using CFD aerodynamics for aeroelastic stability analysis, it was attempted to evaluate the onset of instability directly using a Hopf bifurcation method solving an augmented system for the unknowns $[\boldsymbol{w}, \boldsymbol{x}, \omega, \alpha]$. Variants of Newton's method were applied to solve for the roots of the augmented system. Convergence problems of the Newton iterations related to approximations made when using a direct linear solver[4] were tackled with preconditioned Krylov subspace iterative methods[5] and the application to larger test cases was demonstrated.[6] However, the lack of insight into the development and behaviour of the aeroelastic modes demanded the tracing of eigenvalues as done in conventional (i.e. linear) analyses.

Standard inverse iteration[7] was then applied to iterate to the dominant eigenpair $(\mu, \boldsymbol{x})$ of Eq. (2) to trace aeroelastic eigenvalues with varying α. The well known power method for finding the largest eigenvalue was applied to the shift and invert system $(A - \sigma M)^{-1}$ with the chosen shift σ defining the dominant eigenvalue μ via $(\mu - \sigma)^{-1}$. The shift is usually based on structural frequencies or previously converged solutions,[8] even though this does not guarantee convergence. The algorithm requires the solution of a large, but sparse, linear system, and an iterative linear solver is generally used as direct solvers quickly become prohibitive as the system size increases. The solution of the linear system becomes the inner iteration in an outer inverse iteration process. One of the problems associated with inverse iteration is ill–conditioning of the linear system, increasing with the shift σ approaching μ. Also, in other situations it is simply not known what a good shift σ would be.

Fortunately, for many aeroelastic problems the main interest lies in the development and interaction of the structural modes, and the mathematical arrangement of the coupled system can be exploited. More specifically, the coefficient matrix A generally contains four matrix blocks with the two off–diagonal blocks describing the coupling between fluid and structure. Block Gaussian elimination (with the fluid Jacobian matrix as pivot) gives the so–called Schur complement of the coefficient matrix, and the large linear eigenvalue problem in Eq. (2) becomes a small nonlinear eigenvalue problem of the structural equations corrected for the aerodynamic influence,

$$\{A_{ss} - A_{sf}(A_{ff} - \mu I)^{-1}A_{fs}\}\boldsymbol{x}_s = \mu \boldsymbol{x}_s \tag{3}$$

with subscripts denoting fluid and structure.[9] Essentially, the fluid eigenvector is eliminated from Eq. (2) to give the latter equation. The eigenvalues μ, which we are interested in, are not eigenvalues of the fluid Jacobian matrix A_{ff}. Once the Schur complement formulation was presented, the step of approximating the aerodynamic influence matrix became obvious.[10,11] Using the aerodynamic influence matrix interpolated from numerical samples, stability analyses in multidimensional parameter spaces can be accomplished at the cost of several steady state simulations (provided an efficient algorithm for linear system solves is available and smart *a posteriori* sampling of the parameter space is performed). More importantly, the Schur complement variation of the aeroelastic eigenvalue problem made the approach equivalent to using linear aerodynamic models, such as the doublet lattice method, and work–processes long established in industrial flutter analyses can easily be adapted for the use of CFD methods.

Consider the eigenvalue problem given in Eq. (2) when Schur complement rearrangements are not possible. Existing eigenvalue solvers, such as inverse iteration, work well when eigenvalues of Eq. (2) near a given shift σ are wanted. However, in the computation of the rightmost eigenvalues of Eq. (2), there is in general no robust way to determine a good choice for σ. If the rightmost eigenvalue is real, then $\sigma = 0$ is a good choice; if the rightmost eigenvalues consist of a complex conjugate pair, it is not clear how to choose σ since the imaginary part of critical eigenvalue is unknown. The recently developed Lyapunov inverse iteration[12,13] is able to approximate the critical parameter α_c without the requirement of a good estimate of the critical eigenvalue. Assume that α_0 is a parameter value close to α_c and that the equilibrium solution $\boldsymbol{w}_0(\alpha_0)$ to Eq. (1) at α_0 is stable. It is shown in ref. 12 that the difference $\lambda_c = \alpha_c - \alpha_0$ is the eigenvalue with smallest modulus of an $n^2 \times n^2$ eigenvalue problem with a special Kronecker structure. Once this eigenvalue is known, the critical parameter value α_c can be computed. However, applying inverse iteration directly to the $n^2 \times n^2$ eigenvalue problem is obviously not feasible, since it requires solving linear systems of order n^2, where n is already large when using CFD aerodynamics. Due to its Kronecker structure, this eigenvalue problem can be rewritten in the form of a matrix equation of Lyapunov structure. If we apply inverse iteration to the new problem, we need to solve Lyapunov equations of order n instead, which is feasible. This algorithm is referred to as the Lyapunov inverse iteration. Like the standard inverse iteration, it has an inner–outer structure; the outer iteration is the inverse iteration on the eigenvalue problem of Lyapunov structure, and the inner iteration is solving a Lyapunov equation. In ref. 13, Lyapunov inverse iteration is applied to detect Hopf bifurcations in models of incompressible internal flow (including driven cavity flow and channel flow past an obstacle), and the numerical experiments demonstrate its robustness. Various aspects of the implementation of this algorithm, such as the use of inexact inner iterations and the comparison of different solvers for Lyapunov equations, are discussed in ref. 13 as well.

The paper continues with a more detailed description of the presented inexact Lyapunov inverse iteration followed by an overview of the CFD solvers as well as structural models used. Then, results are presented for the aeroelastic problems of a NACA 0012 aerofoil and the three–dimensional Goland wing/store configuration to approximate the onset of the flutter instability. Results are also shown for the fluid stability problem of a two–dimensional circular cylinder. This paper presents the first use of the Lyapunov inverse iteration method for aeroelastic and compressible flow stability problems.

II. Lyapunov Inverse Iteration

We are interested in the direct computation of the instability onset through a Hopf bifurcation when the physical parameter α takes a critical value. Let the Jacobian matrix of Eq. (1) evaluated at the equilibrium solution $\boldsymbol{w}_0(\alpha)$ be

$$\mathcal{J}(\alpha) = \frac{\partial \boldsymbol{f}}{\partial \boldsymbol{w}}(\boldsymbol{w}_0(\alpha), \alpha) = \frac{\partial \boldsymbol{f}}{\partial \boldsymbol{w}}(\alpha). \tag{4}$$

Assume the point $(\alpha_0, \boldsymbol{w}_0(\alpha_0))$ is in the stable regime and it is close to the critical point $(\alpha_c, \boldsymbol{w}_0(\alpha_c))$. If $\lambda_c = \alpha_c - \alpha_0$, then the Jacobian matrix $\mathcal{J}(\alpha_c)$ can be approximated by a Taylor series as $A + \lambda_c B$, where $A = \mathcal{J}(\alpha_0)$ and $B = \frac{d\mathcal{J}}{d\alpha}(\alpha_0)$. Matrices A and B are large, sparse and nonsymmetric, and B can also be singular. Assume that the stability of $\boldsymbol{w}_0(\alpha)$ is lost through Hopf bifurcation and that the critical eigenpairs at the Hopf point $(\alpha_c, \boldsymbol{w}_0(\alpha_c))$ are $(i\omega_c, \boldsymbol{x}_c)$ and $(-i\omega_c, \overline{\boldsymbol{x}}_c)$, where $\overline{\boldsymbol{x}}$ is complex conjugate to $\boldsymbol{x}$ and $\omega_c > 0$. The rightmost complex conjugate pair of eigenvalues is purely imaginary. Then λ_c is the parameter value closest to zero such that the parameterised eigenvalue problem

$$(A + \lambda B)\boldsymbol{x} = \mu M \boldsymbol{x} \tag{5}$$

has a pair of eigenvalues that sum to zero. Following ref. 13, when M is nonsingular, this is equivalent to a related problem; λ_c is the value of λ closest to zero such that the $n^2 \times n^2$ matrix

$$(A + \lambda B) \otimes M + M \otimes (A + \lambda B) \tag{6}$$

has a double zero eigenvalue associated with the eigenvector $\boldsymbol{z}_c = \xi_1 \boldsymbol{x}_c \otimes \overline{\boldsymbol{x}}_c + \xi_2 \overline{\boldsymbol{x}}_c \otimes \boldsymbol{x}_c$, for any $\xi_1, \xi_2 \in \mathbb{C}$. In other words, λ_c is the eigenvalue of

$$(A \otimes M + M \otimes A)\boldsymbol{z} = \lambda(-B \otimes M - M \otimes B)\boldsymbol{z} \tag{7}$$

with smallest modulus corresponding to the parameter α_c closest to the stable point α_0, and the eigenvector associated with it is $\boldsymbol{z}_c$. Once λ_c has been calculated, then α_c can be estimated easily as $\alpha_0 + \lambda_c$. One could apply inverse iteration to Eq. (7) to compute λ_c, but this approach is not feasible since we need to solve linear systems of order n^2. Alternatively, using properties of Kronecker products instead, we can rewrite the $n^2 \times n^2$ eigenvalue problem in Eq. (7) in the form of a matrix equation,[12]

$$AZM^T + MZA^T = \lambda(-BZM^T - MZB^T), \tag{8}$$

where $Z \in \mathbb{C}^{n \times n}$. The two eigenvalue problems in Eqs. (7) and (8) are related by $\boldsymbol{z} = vec(Z)$ (i.e. the columns of the $n \times n$ matrix Z stacked on top of one another give the n^2 vector $\boldsymbol{z}$). The eigenvalue of Eq. (8) with smallest modulus is λ_c, and it has a unique (up to a scalar multiplier), real, symmetric and rank–2 eigenvector $Z_c = \boldsymbol{x}_c \boldsymbol{x}_c^* + \overline{\boldsymbol{x}}_c \boldsymbol{x}_c^T$. This eigenvector has a low–rank representation $\mathcal{V}\mathcal{D}\mathcal{V}^T$, where $\mathcal{V} \in \mathbb{R}^{n \times 2}$ is orthonormal and $\mathcal{D} \in \mathbb{R}^{2 \times 2}$ is diagonal, and the columns of $\mathcal{V}$ span $\{\boldsymbol{x}_c, \overline{\boldsymbol{x}}_c\}$. Motivated by computational cost, it is suggested in ref. 13 to look at an equivalent eigenvalue problem

$$SZ + ZS^T = \lambda(-TZS^T - SZT^T) \tag{9}$$

where $S = A^{-1}M$ and $T = A^{-1}B$. (Note that Eq. (9) is obtained by left– and right–multiplying Eq. (8) by A^{-1}.) At each step of inverse iteration applied to Eq. (9), we need to solve a large–scale Lyapunov equation

$$SY_j + Y_j S^T = -TZ_j S^T - SZ_j T^T \tag{10}$$

for Y_j, where Z_j is the real and symmetric eigenvector iterate that will converge to Z_c as inverse iteration proceeds. Since n is large, direct methods for solving Lyapunov equations are not practical and applying an iterative solver to Eq. (10) is the only option. For iterative Lyapunov solvers, it is desirable that the right–hand side of Eq. (10) is of low rank. Since $rank(TZ_jS^T + SZ_jT^T) = 2 \cdot rank(Z_j)$, we prefer that the iterates always have a low rank. Although Z_j will eventually converge to the rank–2 target eigenvector Z_c, before convergence Z_j can still have a rank much higher than 2. To address this issue, a rank–reduction process is introduced in ref. 12 to guarantee that Z_j is always of rank 2 (i.e. $Z_j = \mathcal{V}_j \mathcal{D}_j \mathcal{V}_j^T$ where $\mathcal{V}_j \in \mathbb{R}^{n \times 2}$ is orthonormal and $\mathcal{D}_j \in \mathbb{R}^{2 \times 2}$ is diagonal). Since $rank(Z_j) = 2$, the right–hand side in Eq. (10) will always be rank–4. We can obtain estimates for $(\mu_j, \boldsymbol{x}_j)$ as byproducts of Lyapunov inverse iteration by solving the 2×2 eigenvalue problem

$$\mathcal{V}_j^T (A + \lambda_j B)\mathcal{V}_j \boldsymbol{y} = \mu_j \mathcal{V}_j^T M \mathcal{V}_j \boldsymbol{y}. \tag{11}$$

The estimated eigenvector is $\boldsymbol{x}_j = \mathcal{V}_j \boldsymbol{y}$ and the estimated eigenvalue is μ_j. Since $\mathcal{V}_j$ converges to $\mathcal{V}$ and the columns of $\mathcal{V}$ span $\{\boldsymbol{x}_c, \overline{\boldsymbol{x}}_c\}$, the estimate $(\mu_j, \boldsymbol{x}_j)$ converges to the true eigenpair $(\mu_c, \boldsymbol{x}_c)$.

We apply the Krylov method as described in ref. 14 to solve the Lyapunov equation in Eq. (10). The solution Y_j computed by the Krylov method in factored form is $Y_j = V_j D_j V_j^T$ where $V_j \in \mathbb{R}^{n \times m_j}$ is orthonormal and $D_j \in \mathbb{R}^{m_j \times m_j}$ is diagonal. The rank of the solution without truncation denoted m_j also indicates the approximate number of linear solves with the matrix A needed to obtain this solution.

As observed in the numerical experiments in ref. 13, solving Eq. (10) accurately can be extremely difficult in the early stages of inverse iteration. As the inverse iteration proceeds, this becomes progressively easier. The following strategy is then proposed in ref. 13. We solve the Lyapunov equation in Eq. (10) such that its residual norm is proportional to the residual norm of the eigenvalue problem in Eq. (9), namely,

$$\|R_j\|_F \leq \delta \|\mathfrak{R}_j\|_F, \tag{12}$$

where $\delta > 0$ is a constant, $R_j = SY_j + Y_j S^T + TZ_j S^T + SZ_j T^T$ is the residual of the Lyapunov equation in Eq. (10) and $\mathfrak{R}_j = SZ_j + Z_j S^T + \lambda_j (TZ_j S^T + SZ_j T^T)$ is the residual of the eigenvalue problem in Eq. (9). Note that the Frobenius norm of both residuals is cheap to compute. This stopping criterion is adapted from previous studies (e.g. in ref. 15) on inexact inner solves of inverse iteration applied to the eigenvalue problem in Eq. (2). In the early stage of inverse iteration, since (λ_j, Z_j) has not converged to the true eigenpair (λ_c, Z_c) yet (i.e. $\|\mathfrak{R}_j\|_F$ is large), we do not need to solve Eq. (10) accurately either. However, as (λ_j, Z_j) converges, we then solve Eq. (10) more accurately. In the current study, the values of the chosen δ are all between 10^{-4} and 10^{-2}, depending on the problem.

III. Flow and Structural Models

Different flow solvers are used for this study. In contrast to the earlier papers on Lyapunov inverse iteration, we are looking at external flow using codes solving the compressible form of the governing equations. The aerodynamics of the aeroelastic aerofoil and wing problems is modelled by the Euler equations. The flow equations are solved using a block–structured, cell–centred, finite–volume scheme for spatial discretisation. Convective fluxes are evaluated by an approximate Riemann solver with the MUSCL scheme achieving higher–order accuracy and van Albada's limiter maintaining a monotone solution around steep gradients. At wall boundaries the slip condition is enforced, while far field boundaries assume freestream conditions. Steady state solutions are found using implicit time–marching in pseudo time, while unsteady time–accurate simulations employ the standard dual time stepping approach. Linear systems resulting from the implicit approach are solved using a preconditioned Krylov subspace iterative algorithm. The exact fluid Jacobian matrix corresponding to the spatial scheme is evaluated analytically and stored explicitly. Details on various aspects of the flow solver and the evaluation of the fluid Jacobian matrix can be found, for instance, in refs. 2 and 16.

For the aeroelastic test cases, standard structural models are used. The aerofoil problem uses a two–degrees–of–freedom pitch and plunge model as described, for instance, in ref. 17. The independent parameter is the reduced velocity as a dimensionless representation of the freestream velocity. The isolated wing problem uses a modal structural model where the linear structural deformation is found by superposition of the fundamental deformations. These mode shapes are available from an analysis of the finite element description of the wing structure. For the wing problem, the aeroelastic modes are traced with respect to the altitude in a matched point fashion using a standard atmosphere model. Equation (5) for the aeroelastic problems can be written in partitioned form as,

$$\left\{ \begin{pmatrix} A_{ff} & A_{fs} \\ A_{sf} & A_{ss} \end{pmatrix} + \lambda \begin{pmatrix} B_{ff} & B_{fs} \\ B_{sf} & B_{ss} \end{pmatrix} \right\} \boldsymbol{x} = \mu M \boldsymbol{x} \tag{13}$$

where the eigenvector $\boldsymbol{x}$ contains fluid and structural contributions according to the matrices. The matrix M in the general formulation of the eigenvalue problem becomes the identity matrix for the finite volume discretisation of the Euler flow equations in the multiblock code. In both cases, the Jacobian matrix of the structural equations is exact, while the matrix blocks expressing the coupling between fluid and structure (i.e. the dependence of the fluid equations on the structural unknowns and vice versa) are evaluated from finite differences. As we are considering symmetric aeroelastic test cases where the structural equilibrium solution is trivial (i.e. no static deformation), there is no dependence of the fluid residual on the independent parameter α. Thus, the matrix blocks B_{ff} and B_{fs} are zero. Additionally for the aerofoil problem, the matrix block B_{sf} is zero as α is chosen to be the reduced velocity. The evaluation of the matrix block B_{ss} is

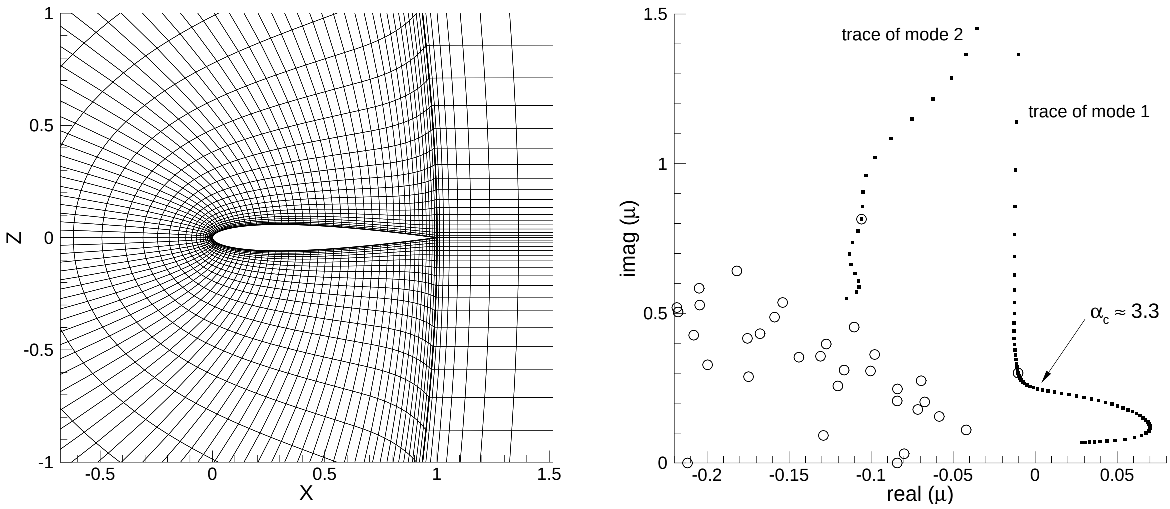

(a) Block–structured NACA 0012 aerofoil mesh.

(b) Mode traces using $\Delta\alpha = 0.05$ and representative eigenvalue spectrum (open circles) at $\alpha = 2.5$.

Figure 1. NACA 0012 aerofoil test case.

done analytically. For the wing, α is chosen to be the altitude (with the modes being traced with decreasing values of α) thus influencing the structural residual through the dynamic pressure giving a nonzero block B_{sf}. Both nonzero matrix blocks are evaluated by finite differences using an increment of $\Delta\alpha = 100$ ft. Steady state simulations are all converged ten orders of magnitude relative to the initial residual norm.

For fluid–only problems, compressible viscous flow is assumed. The Navier–Stokes equations are solved using a meshless spatial discretisation scheme in a newly developed research code. Spatial derivatives are approximated using a least squares method working on clouds of points distributed throughout the computational domain. Similar to the multiblock code, convective fluxes are evaluated by Osher's approximate Riemann solver where a continuously differentiable MUSCL–type scheme is used to give the higher–order accurate left and right state flow variables[18] while van Albada's limiter maintains a monotone solution around steep gradients. Viscous fluxes are evaluated using (modified) averages of flow variables and their gradients at the half way point between neighbours. At wall boundaries the no–slip condition is strongly enforced, while at far field boundaries the flow is assumed to return to freestream conditions. The methods used for converging to steady state solutions as well as for performing unsteady, time–accurate simulations follow the multiblock code as described above. Details on the meshless flow solver can be found in ref. 19.

The fluid Jacobian matrix is evaluated exactly using analytical derivatives of the residuals. The independent parameter α is chosen to be the Reynolds number. This choice gives a matrix B with a sparsity pattern similar to the Jacobian matrix A as all equations of the Navier–Stokes flow model, except for the continuity equation, depend on Reynolds number. The matrix B is formed using finite differences with a chosen increment of $\Delta\alpha = 0.1$. As for the aeroelastic cases, the steady state convergence criterion is ten orders of magnitude less than the initial residual.

IV. Aeroelastic Stability Results

Results are presented for two problems. Inexact Lyapunov inverse iteration is first applied to the two–degrees–of–freedom pitch and plunge aerofoil model using the NACA 0012 profile, and then the Goland wing/store configuration with four aeroelastic modes is investigated. We are interested in approximating the critical eigenpair for the coupled fluid/structural system without prior information, which could then be used in further analysis, such as in standard inverse iteration with a good idea on the choice of the required shift σ (and also on the important initial guess for the relevant eigenvector) or in nonlinear reduced order models[20] to exploit the critical eigenspace for an investigation into a limit cycle amplitude.

The computational mesh used for the NACA 0012 aerofoil simulations is shown in figure 1(a). The domain is discretised with 4,096 control volumes (resulting in $16,388$ as the dimension of the eigenvalue

Table 1. NACA 0012 aerofoil results; $\alpha_0 = 2.50$, $\delta = 10^{-2}$.

j	α_j	μ_j	$\|\boldsymbol{r}_j\|_2$	$\|\mathfrak{R}_j\|_F$	$\|R_j\|_F$	m_j
1	-613.832	-9.09237	1.61606e+02	6.60938e+03	6.75160e−01	2
2	3.42750	0.00000	2.80976e−04	4.35758e−02	4.10259e−04	88
3	3.03527	0.24725i	3.89835e−03	3.61728e−03	2.71849e−05	96
4	3.04999	0.25020i	3.89835e−05	2.81842e−05	2.40013e−07	112
5	3.04979	0.25018i	9.78046e−07	8.09191e−07	6.17044e−09	120
6	3.04980	0.25018i	3.32597e−08	2.10498e−08	1.88826e−10	100
7	3.04980	0.25018i	4.77404e−10	8.25394e−10	—	—

Table 2. NACA 0012 aerofoil results; $\alpha_0 = 2.50$, $\delta = 10^{-4}$.

j	α_j	μ_j	$\|\boldsymbol{r}_j\|_2$	$\|\mathfrak{R}_j\|_F$	$\|R_j\|_F$	m_j
1	-613.832	-9.09237	1.61606e+02	6.60938e+03	9.92762e−02	4
2	3.43115	0.00071	2.54687e−04	4.26639e−02	4.05236e−06	180
3	3.04781	0.25073i	1.67038e−03	8.45098e−04	8.13249e−08	284
4	3.04979	0.25018i	1.00406e−05	3.03776e−06	2.93925e−10	228
5	3.04980	0.25018i	1.05765e−08	6.52864e−09	5.79518e−13	208
6	3.04980	0.25018i	8.78967e−10	6.53550e−09	—	—

Table 3. NACA 0012 aerofoil results; $\alpha_0 = 3.05$, $\delta = 10^{-2}$, solution of $\alpha_0 = 2.5$ as initial guess to eigenvector.

j	α_j	μ_j	$\|\boldsymbol{r}_j\|_2$	$\|\mathfrak{R}_j\|_F$	$\|R_j\|_F$	m_j
1	3.30354	0.25018i	1.03152e−09	8.26346e−08	5.83777e−10	72
2	3.30354	0.25018i	4.51451e−10	1.01488e−09	—	—

problem). The structural parameters for the two–degrees–of–freedom pitch and plunge aerofoil model were given in ref. 5. The flutter analysis is done for the low transonic Mach number of 0.75 and zero degrees angle–of–attack. In figure 1(b) a detail around the origin of a representative eigenvalue spectrum for $\alpha = 2.5$, calculated using Matlab routines, is presented together with the development of the two aeroelastic modes with increasing values of α (representing the reduced velocity). The increment used for the tracing is $\Delta\alpha = 0.05$. The eigenvalue traces were computed using the Schur complement formulation of the eigenvalue problem as described above. Details on the calculation of these reference data can be found, for instance, in ref. 10. It can clearly be seen that the mode traces, when reaching $\alpha = 2.5$, match with two eigenvalues of the spectrum. The results of the Schur complement approach are taken as reference when discussing the Lyapunov inverse iteration. From the figure it can be seen that the eigenvalues originating in the matrix A_{ss} are well apart from the dense group of fluid eigenvalues when α is low. With increasing α the structural eigenvalues approach the fluid group indicating the stronger fluid/structural interaction which eventually results in flutter. The critical parameter value α_c is approximately 3.3 while the (dimensionless) circular frequency ω_c at flutter onset is approximately 0.25.

The tables presented in this paper to show the performance of the Lyapunov approach require some explanation. The first three columns are the outer iteration number j, the predicted (critical) parameter value α_j and the corresponding (rightmost) eigenvalue $\mu_j = i\omega_j$. The eigenvalue estimate μ_j (and also the eigenvector $\boldsymbol{x}_j$) are found as solution from Eq. (11). The expression $\|\boldsymbol{r}_j\|_2$ gives the norm of the residual of Eq. (5) with $\boldsymbol{r}_j = (A + \lambda_j B)\boldsymbol{x}_j - \mu_j \boldsymbol{x}_j$ where $\lambda_j = \alpha_j - \alpha_0$. The next two columns give the Frobenius norm of the eigenvalue problem in Eq. (9) and of the Lyapunov equation in Eq. (10), respectively. Note that the Lyapunov equation is only solved to an accuracy relative to the solution of the eigenvalue problem indicated by δ in Eq. (12). The column for m_j (i.e. the rank of the solution of the Lyapunov equation without truncation) indicates the main computational work. The value of m_j gives the approximate number of linear system solves with coefficient matrix A required by the approach.

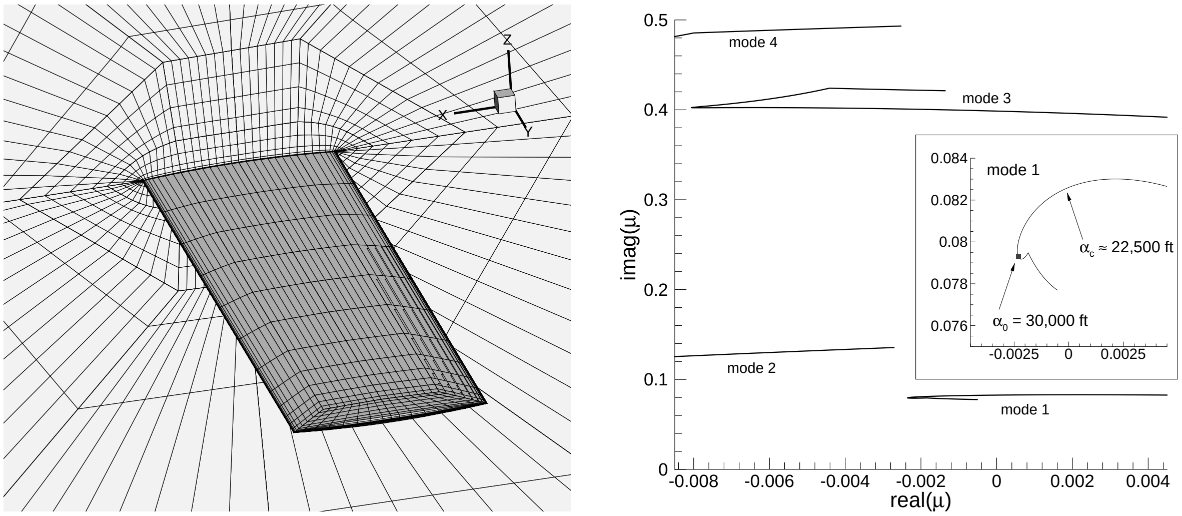

(a) Block–structured Goland wing mesh.

(b) Mode traces for four aeroelastic modes; inner frame shows magnified first mode.

Figure 2. Goland wing/store test case.

Tables 1 through 3 show the results for the aerofoil problem. The stopping criterion used for the aerofoil calculations is $\|r_j\|_2 < 10^{-9}$ throughout. The results in tables 1 and 2 are obtained using matrices A and B evaluated at $\alpha = 2.5$, the corresponding eigenvalue spectrum of which can be found in figure 1(b). Three to four outer iterations are sufficient to find the solution with an acceptable level of convergence. The non–physical critical parameter value at the first iteration is due to the randomly chosen (non–physical) eigenvector to initialise the solution. From the second iteration, the solution quickly converges to meaningful results. The computational cost as indicated by m_j is rather high, particularly comparing with the results for the Goland wing/store configuration given below. Decreasing the parameter δ for the inexact Lyapunov solves from 10^{-2} to 10^{-4} approximately doubles the number of linear system solves required. However, the more accurate solution of the Lyapunov equation does not speed up the outer convergence significantly when comparing the outer iteration count.

The same test was performed using matrices evaluated at $\alpha_0 = 1.5$, the convergence results of which are not presented. For $\alpha_0 = 1.5$, as can be derived from figure 1(b), the relevant eigenvalue (i.e. the bending mode) is clearly located before the deflection of the trace towards the imaginary axis. The test did not give a converged solution. This can be explained considering the underlying first order Taylor expansion of the Jacobian matrix in Eq. (5) where the derivative of the matrix A indicates an eigenvalue trace almost parallel to the imaginary axis. From a physical point of view, for the Lyapunov approach to be successful the dominant mechanism eventually causing the instability needs to be found and represented in the Jacobian matrix. In the case of the aerofoil flutter instability, this requires that a strong interaction of bending and torsion modes, and consequently frequency coalescence, is well resolved.

The final set of data for the aerofoil problem is provided in table 3 to demonstrate the importance of having a good starting solution for the eigenvector. The choice of $\alpha_0 = 3.05$ is based on the predicted critical parameter from the analysis at $\alpha_0 = 2.5$. An analysis starting with a randomly chosen eigenvector gives a performance similar to the first two tables for $\alpha_0 = 2.5$. The calculation converges to the correct critical parameter and frequency. Using the previously calculated eigenvector as starting solution however, the solution is found immediately as seen in table 3.

The second test problem is now discussed. The Goland wing is a model wing having a chord of 6 ft and a span of 20 ft. It is rectangular and cantilevered with a constant cross section defined by a 4% thick symmetric parabolic–arc aerofoil. The wing tip is rounded. The computational mesh used for the simulations of the Goland wing/store configuration is shown in figure 2(a). The store aerodynamics are not modelled. The domain is discretised with 24,192 control volumes, giving $120,968$ as the dimension of the eigenvalue problem. These are the five fluid variables per cell plus the structural unknowns for the four normal modes. The normal mode frequencies are 1.689, 3.051, 9.173 and 10.83 (all given in Hz). Structural damping is neglected. The

Table 4. Goland wing/store results; $\alpha_0 = 30,000$ ft, $\delta = 10^{-4}$.

j	α_j	μ_j	$\|\boldsymbol{r}_j\|_2$	$\|\mathfrak{R}_j\|_F$	$\|R_j\|_F$	m_j
1	-1.59e+8	-41.9034	1.12903e+03	5.45301e+03	1.55669e−05	2
2	-23,514.4	-0.00000	7.07420e−03	4.37023e+00	7.72942e−06	8
3	15,623.3	0.08843i	1.21917e−02	1.03323e−01	6.95630e−06	4
4	21,584.7	0.07643i	2.43377e−03	4.76802e−02	1.72526e−06	12
5	22,293.0	0.08328i	3.49511e−04	7.17590e−03	5.17148e−07	12
6	22,090.7	0.08260i	1.19861e−04	3.17729e−03	4.96654e−08	16
7	22,071.8	0.08223i	1.56751e−05	2.70952e−04	2.12832e−08	16
8	22,077.7	0.08224i	7.16958e−06	1.22351e−04	—	—

Table 5. Goland wing/store results; $\alpha_0 = 22,078$ ft, $\delta = 10^{-4}$, solution of $\alpha_0 = 30,000$ ft as initial guess to eigenvector.

j	α_j	μ_j	$\|\boldsymbol{r}_j\|_2$	$\|\mathfrak{R}_j\|_F$	$\|R_j\|_F$	m_j
1	22,551.3	0.08232i	2.86017e−05	8.93826e−03	3.36599e−07	8
2	22,567.2	0.08260i	4.30505e−06	7.42594e−05	—	—

finite–element model, used to calculate the mode shapes, follows the description given in ref. 21. The flutter analysis is done for the high subsonic Mach number of 0.85 and zero degrees angle–of–attack.

In figure 2(b) the traces of the four relevant modes for decreasing values of α (representing the altitude) are shown. These reference results were computed using the Schur complement formulation of the eigenvalue problem as described above. The flutter instability follows from the typical wing bending–torsion coupling in the first (bending) and second (torsion) mode. The critical parameter value α_c is approximately 22,500 ft while the (dimensionless) frequency ω_c at flutter onset is approximately 0.0826. A second instability is encountered in the third mode at lower altitudes (which is thus less important from a general stability point of view) of about 10,300 ft following the interaction of the two higher modes.

Tables 4 and 5 present the results for the wing case. The stopping criterion used is $\|\boldsymbol{r}_j\|_2 < 10^{-5}$, while the value of δ is set to 10^{-4}. The results in table 4 are obtained using matrices A and B evaluated at $\alpha = 30,000$ ft. As for the aerofoil problem, the non–physical critical parameter value at the first two iterations is due to the randomly chosen (non–physical) eigenvector to initialise the solution. From the third iteration, quick convergence is observed. Comparing table 4 for the wing and table 2 for the aerofoil problem, it is found that the rank m_j of the Lyapunov solution (i.e. the cost of the iterations) is significantly higher for the aerofoil even though, in both cases, inviscid Euler flow is assumed and thus the eigenvalue spectrum is expected to be similar. The reason behind this observation is currently not understood, and more insight will be required in future work to clarify these differences.

Similar to the aerofoil study, a second iteration is done with the system matrices A and B evaluated at $\alpha_0 = 22,078$ ft which is the predicted critical parameter value α_c found in table 4. Note that $\alpha_0 = 22,078$ ft corresponds to an unstable test point. The flow equations however are solved without updating the structural solution. The structural equilibrium remains the trivial solution. These results are presented in table 5. The good starting solution for the eigenvector results in rapid convergence as expected.

As was indicated above, the prime application of Lyapunov inverse iteration are not aeroelastic problems where eigenvalues of the structural system are well separated from fluid eigenvalues providing the shift σ immediately from the normal mode frequencies. The aeroelastic stability analysis using CFD aerodynamics is (arguably) most efficiently and robustly done in terms of the Schur complement formulation with the aerodynamic influence, correcting an otherwise structure–only eigenvalue problem, approximated from samples using kriging interpolation or other means of constructing response surfaces. Knowledge of the development and interaction of the structural modes at pre–flutter conditions is found and this information is important to the analyst. Lyapunov inverse iteration, on the other hand, would provide estimates of the critical eigenspace without tracing the modes, while no estimate to the shift is required. A more relevant application of the Lyapunov approach is discussed in the next section.

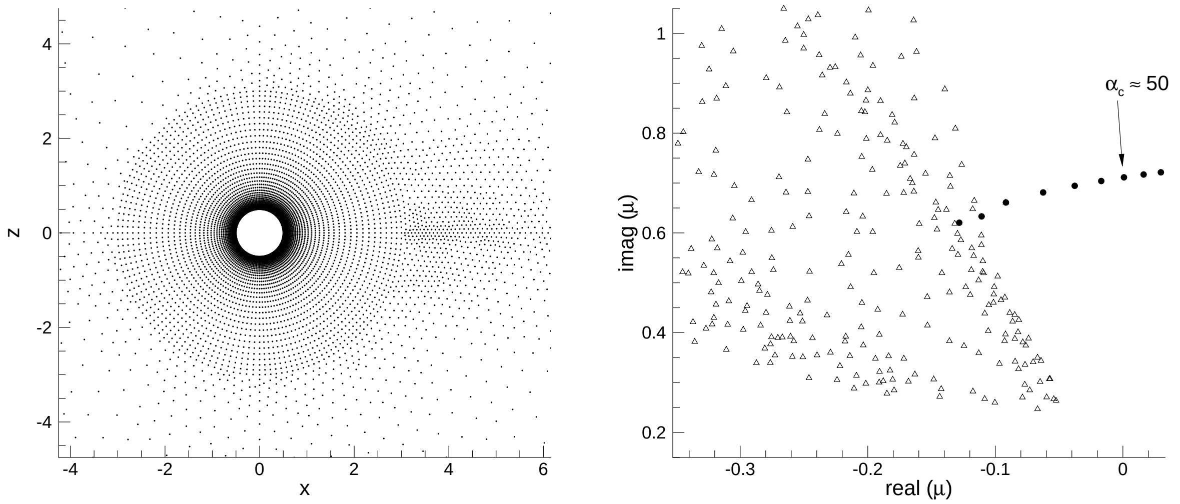

(a) Point distribution around cylinder.

(b) Mode trace using $\Delta\alpha = 5$ and representative eigenvalue spectrum (triangles) at $\alpha = 30$.

Figure 3. Circular cylinder test case.

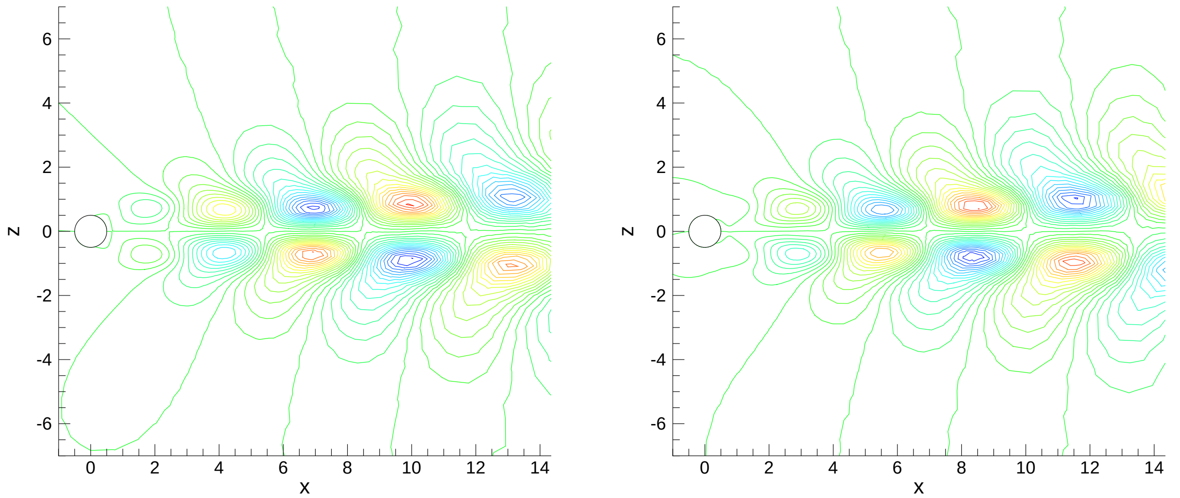

(a) Real part.

(b) Imaginary part.

Figure 4. Critical eigenvector x_c at $\alpha = 50$ showing contours of x–velocity component.

V. Fluid Stability Problem

The flow solutions for the discussion of the fluid–only stability problem are simulated using a recently developed meshless solver.[19] The computational domain of the two–dimensional circular cylinder is discretised with 10,951 points giving $43,804$ as the dimension of the eigenvalue problem for the four fluid variables per point. The coarse point distribution used for the cylinder simulations is shown in figure 3(a). The points were taken from a mesh, which is structured close to the cylinder surface (with a minimum wall–normal spacing of $2 \times 10^{-3}d$ where d is the characteristic cylinder diameter) and unstructured with triangular elements beyond three cylinder diameters distance from the origin. The domain extends 125 diameters to the far field. The stencil for each point in the domain is based on the original connectivity of the underlying mesh. The analysis is done for the subsonic Mach number of 0.2 as presented in an earlier numerical study on global stability analysis in ref. 22. As said above, the independent parameter α is chosen to be the Reynolds number.

Table 6. **Circular cylinder results; $\alpha_0 = 30$, $\delta = 10^{-3}$.**

j	α_j	μ_j	$\|\boldsymbol{r}_j\|_2$	$\|\mathfrak{R}_j\|_F$	$\|R_j\|_F$	m_j
1	180.321	-225.663	2.82941e+05	1.44442e+03	7.71734e−01	6
2	121.867	0.04577	1.53087e+01	2.76004e+01	2.09574e−02	20
3	73.2355	0.18464	1.33241e+01	5.58908e+00	5.23180e−03	120
4	58.2050	1.00357	4.19155e+02	2.91294e+00	2.39466e−03	444
5	39.7731	0.58968i	2.44273e+02	1.63539e−01	1.51410e−04	408
6	42.9995	0.84511i	1.08419e+02	6.42432e−02	5.69698e−05	456
7	44.2268	0.75871i	5.39117e+01	1.12070e−02	5.34444e−05	600*
8	44.1682	0.75163i	2.10807e+01	7.72277e−02	6.51478e−05	200
9	44.1659	0.74556i	1.30318e+01	2.14273e−03	2.04979e−06	360
10	44.1545	0.74334i	4.47845e+00	3.12377e−04	2.74946e−07	512
11	44.1510	0.74180i	2.15854e+00	7.72622e−02	6.73597e−05	80
12	44.1507	0.74124i	1.37384e+00	1.93762e−04	1.79126e−07	344
13	44.1506	0.74094i	4.74067e−01	2.97421e−05	2.87677e−08	372
14	44.1508	0.74080i	2.87344e−01	1.15115e−04	1.12520e−07	256
15	44.1507	0.74074i	1.43780e−01	6.23599e−06	6.00802e−09	344
16	44.1508	0.74071i	5.00196e−02	8.99418e−06	8.09050e−09	264
17	44.1508	0.74069i	2.77117e−02	1.58366e−06	1.45289e−09	324
18	44.1508	0.74068i	1.15913e−02	1.35034e−04	1.24811e−07	84
19	44.1508	0.74068i	6.52256e−03	9.40074e−07	—	—

* Krylov method failed to converge to desired tolerance. Maximum number of Krylov vectors allowed is 600.

At the critical Reynolds number, the flow around the cylinder encounters an instability which results in the shedding of vortices in the wake behind the cylinder. In ref. 23 the critical Reynolds number of the onset of laminar vortex shedding is stated to be about 49, while in ref. 22 it is numerically predicted to be about 47. The Strouhal number St at critical conditions is stated to be about 0.12 in various numerical and experimental studies.[22–24] This Strouhal number translates to a critical (dimensionless) frequency of about 0.75. In the current investigation, we find instability onset at $\alpha_c \approx 50$ with a shedding frequency of about 0.72. These are good estimates within range. A spatial convergence study is not attempted in the current work. In addition, time–accurate simulations, the results of which are not presented, agree with the eigenvalue stability analysis. These simulations used a (dimensionless) real time step of 0.02 while converging the solution three orders of magnitude in pseudo time. Two simulations at Reynolds numbers of 49 and 51 indicated decaying and growing amplitudes, respectively, while a Reynolds number of 50 gave oscillating lift, drag and moment coefficients with a nearly constant amplitude and a circular frequency matching the eigenvalue results.

In figure 3(b) a detail around the origin of the eigenvalue spectrum for $\alpha = 30$, calculated using Matlab routines, is presented together with the development of the relevant eigenvalue with increasing α. The eigenvalue trace is shown for Reynolds numbers between 20 and 60 using an increment of $\Delta\alpha = 5$. From the figure it can be seen that one eigenvalue, emerging from a dense group of eigenvalues, moves towards the imaginary axis as α is increased towards critical conditions. For visualisation purposes, in figure 4 the eigenvector $\boldsymbol{x}_c$ at the instability onset for $\alpha_c = 50$ is plotted. The contour lines of the real and imaginary parts of the x–velocity component are shown indicating the vortex shedding. Interestingly, in figure 3(b) the eigenvalue trace describes an almost straight line which suggests the Taylor expansion $A + \lambda B$ is a good approximation (keeping in mind, however, that the Taylor expansion is applied to the matrix elements and not the eigenvalue itself). It is also obvious that for lower values of α a good choice for the shift σ (to be used, for instance, in standard inverse iteration) is difficult to provide. This is the situation when the Lyapunov approach is required; to pull the relevant eigenvalue out from a dense group of eigenvalues while giving an estimate of the instability onset.

Table 7. Circular cylinder results; $\alpha_0 = 40$, $\delta = 10^{-3}$.

j	α_j	μ_j	$\Vert \boldsymbol{r}_j \Vert_2$	$\Vert \mathfrak{R}_j \Vert_F$	$\Vert R_j \Vert_F$	m_j
1	256.641	-194.180	2.33523e+05	1.29435e+03	1.24971e+00	4
2	162.208	-0.01007	2.08653e+01	3.02063e+01	2.25373e−02	12
3	94.6532	0.19164	9.62484e+00	4.38880e+00	3.39673e−03	152
4	50.3263	0.66334	1.62947e+02	2.53739e+00	2.51234e−03	508
5	46.2243	0.50070i	4.81667e+02	7.22931e−02	6.92872e−05	492
6	49.0008	0.70591i	7.57497e+01	6.45025e−03	6.05824e−06	488
7	49.0185	0.72726i	2.09232e+01	1.46678e−02	1.42518e−05	320
8	49.0100	0.73244i	4.49475e+00	3.34744e−04	2.62196e−07	460
9	49.0064	0.73358i	1.03154e+00	1.25426e−02	1.24432e−05	56
10	49.0063	0.73383i	2.09367e−01	4.46259e−05	4.37356e−08	400
11	49.0065	0.73389i	4.08395e−02	5.50822e−05	5.11313e−08	300
12	49.0065	0.73390i	1.16318e−02	2.00524e−05	1.89747e−08	220
13	49.0065	0.73391i	2.72913e−03	2.71054e−07	—	—

The convergence results for the cylinder are presented in tables 6 and 7 with the system matrices A and B evaluated at $\alpha_0 = 30$ and $\alpha_0 = 40$, respectively. The stopping criterion used is $\Vert \mathfrak{R}_j \Vert_F < 10^{-6}$. The method converges the solution to a good estimate of the critical conditions even though the convergence behaviour is tight for both the inner and outer iterations. A large number of linear system solves are required as indicated by m_j and the norm of the residual $\boldsymbol{r}_j$ (or equivalently $\mathfrak{R}_j$) decreases slowly. The Lyapunov approach performs somewhat better for the higher Reynolds number of 40 where the relevant eigenvalue is further apart from the dense group as seen in figure 3(b). The reasons behind these rather slow rates of convergence, however, remain to be understood.

Using conventional eigenvalue solvers, on the other hand, one would be faced in general with neither knowing an estimate of λ nor the usually required shift σ. Rather than choosing the shift to be zero, the focus would be directed towards the eigenvalues in the upper half–plane when expecting an instability of the Hopf–type. Thus, a frequency shift (i.e. the imaginary part of the eigenvalue) would be chosen based on engineering intuition. However, the number of eigenvalues closest to the shift, that need to be calculated, is difficult to estimate with limited prior knowledge. In addition, to have an estimate on λ_c several iterations would be required. In figure 3(b), for instance, 300 eigenvalues closest to the shift $\sigma = 0.7\mathrm{i}$ were evaluated, where the shift was chosen based on the expected critical frequency. In this context, the performance of the Lyapunov approach indicates its utility.

Once the numerical difficulties of solving the large scale Lyapunov equations have been understood and overcome, there will, of course, be physical limits to the approach. The (linearised) physics as described by the governing partial differential equations are contained in the Jacobian matrix. When the dominant mechanism for an instability (e.g. the interaction of two modes) is not developed yet, then the Lyapunov approach will fail. This point was suggested by the aerofoil case using $\alpha_0 = 1.5$ as described above. A second example is presented in figure 5. The figure shows the traces of several eigenvalues close to the shift $\sigma = 0.7\mathrm{i}$ for the Reynolds number increasing from 15 to 30 with an increment of $\Delta\alpha = 1$. The critical eigenvalue eventually emerges clearly at the higher Reynolds numbers, while it is not possible to identify the critical one below, say, $\alpha = 25$ by simply inspecting the eigenvalue spectrum. The critical eigenvalue shows an interesting behaviour illustrated in more detail in the inner frame. At a Reynolds number of about 20 the relevant eigenvalue seems to interact with a second eigenvalue resulting in coalescing frequencies. This behaviour is typical for structural modes in aeroelastic applications before the flutter onset.

Using Matlab routines, the eigenvalue problem in Eq. (5) was solved for increasing values of λ to extract parts of the eigenvalue spectrum. The matrices were evaluated at $\alpha_0 = 20$, which is just above the Reynolds number of coalescing frequencies. The critical parameter value was found to be about 35 with a frequency of 0.73. While the frequency estimate is good, the critical parameter is well off. These results show two points. First, as would be expected, to have a good estimate of the critical conditions an equilibrium solution needs to be evaluated in the proximity of the instability onset, where the tolerable value of $\lambda_c = \alpha_c - \alpha_0$ certainly

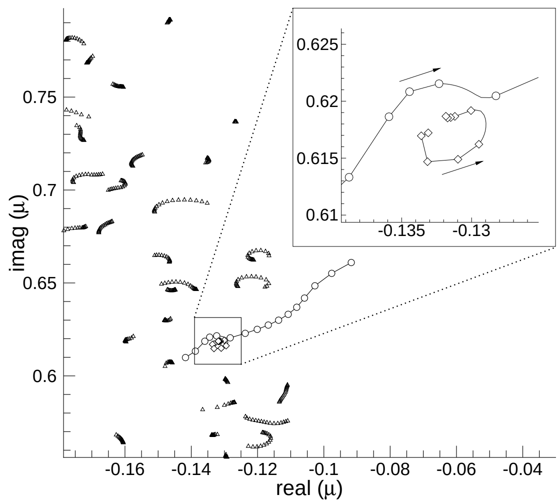

Figure 5. Mode traces using $\Delta\alpha = 1$ for Reynolds numbers between 15 and 30; arrows in inner frame indicate increasing Reynolds number.

depends on the application. Secondly, even though the critical point is not approximated accurately, a good estimate on the critical mode including frequency and eigenvector is provided to guide additional analysis. The critical mode is successfully identified and extracted from the dense group of eigenvalues.

There is another important issue for stability analysis which is not often discussed. In many situations a steady state solution can be simulated, even though the parameter α indicates unstable conditions, due to the use of various convergence acceleration techniques, such as local time stepping or residual smoothing. This is particularly true close to the instability onset. The converged steady state solution would be misleading at this point. If an efficient eigenvalue stability analysis, such as Lyapunov inverse iteration or standard inverse iteration, is then not available, a time–accurate simulation is required which can be become very costly close to the instability onset.

An example is provided in figure 6 for the circular cylinder at different values of Reynolds number. For $\alpha = 30$ the system is stable as discussed earlier, whereas for $\alpha = 100$ we find conditions well inside the unstable (i.e. unsteady) regime. In figure 6(a) three convergence histories are presented. The simulations all start with 200 explicit updates to smooth out the initial flow field before switching to the fully implicit scheme. Using a Courant–Friedrichs–Lewy (CFL) number of 100, the simulations for both values of α converge (at least) ten orders of magnitude without problems. It is observed that the simulation for $\alpha = 100$ has slower convergence compared with the stable test point, which could be interpreted as an indication of unsteadiness in the flow. The time–accurate scheme then predicts the unsteady flow for the higher Reynolds number case. Using the lower CFL number, on the other hand, which effectively gives a smaller (local) pseudo time step, converges the solution initially more than six orders of magnitude. At this point, disturbances in the flow field are amplified even in the steady state solve. In figure 6(b) the oscillatory (steady state) lift coefficient indicates the presence of an unstable mode.

VI. Conclusion

Inexact Lyapunov inverse iteration is presented for stability analysis using computational fluid dynamics. The Lyapunov approach is a recently developed eigenvalue solver which allows the calculation of an estimate of the critical eigenspace as well as the critical independent parameter value using the information provided at an equilibrium point in the vicinity of the instability onset. The only required inputs to the method are the Jacobian matrix of the dynamical system and its derivative with respect to the independent parameter. A shift to the relevant eigenvalue, as needed by standard inverse iteration, is not required.

The method is presented for two aeroelastic cases, including a NACA 0012 pitch and plunge aerofoil and the Goland wing/store configuration, and the fluid stability problem of a circular cylinder. While the aeroelastic configurations assume inviscid compressible Euler flow solved by a structured finite–volume code,

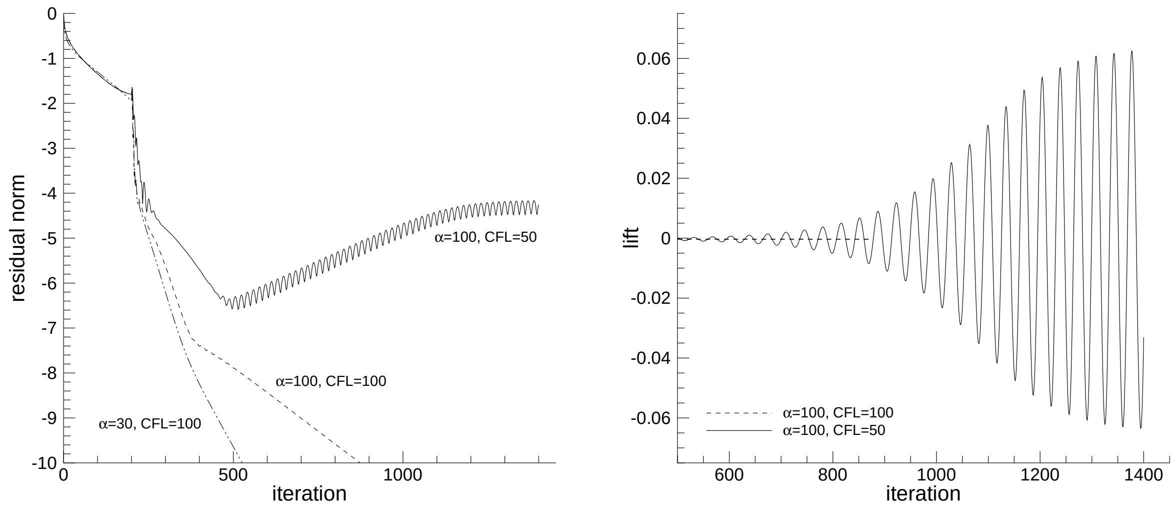

(a) Scaled residual norm. (b) Lift coefficient due to pressure.

Figure 6. Steady state convergence for circular cylinder test case.

the laminar viscous cylinder flow is simulated by a newly developed research code with meshless spatial discretisation. All test cases encounter instability of the Hopf–type, and the critical conditions are predicted by the Lyapunov approach. The results are promising for a future investigation into efficiency and robustness improvements when solving large scale Lyapunov equations as well as for the discussion of specific stability problems, such as shock buffet which would be a prime application of the presented approach.

References

[1]Dowell, E. H. and Hall, K. C., "Modelling of fluid–structure interaction," *Ann. Rev. Fluid Mech.*, Vol. 33, 2001, pp. 445–490.

[2]Woodgate, M. A. and Badcock, K. J., "Fast prediction of transonic aeroelastic stability and limit cycles," *AIAA Journal*, Vol. 45, No. 6, 2007, pp. 1370–1381.

[3]Badcock, K., Khodaparast, H., Timme, S., and Mottershead, J., "Calculating the influence of structural uncertainty on aeroelastic limit cycle response," *AIAA Paper 2011–1741*, 2011.

[4]Morton, S. A. and Beran, P. S., "Hopf–bifurcation analysis of airfoil flutter at transonic speeds," *Journal of Aircraft*, Vol. 36, No. 2, 1999, pp. 421–429.

[5]Badcock, K. J., Woodgate, M. A., and Richards, B. E., "Hopf bifurcation calculations for a symmetric airfoil in transonic flow," *AIAA Journal*, Vol. 42, No. 5, 2004, pp. 883–892.

[6]Badcock, K. J., Woodgate, M. A., and Richards, B. E., "Direct aeroelastic bifurcation analysis of a symmetric wing based on Euler equations," *Journal of Aircraft*, Vol. 42, No. 3, 2005, pp. 731–737.

[7]Golub, G. H. and van Loan, C. F., *Matrix computations*, John Hopkins University Press, Baltimore, MD, 3rd ed., 1996.

[8]Badcock, K. J., Timme, S., Marques, S., Khodaparast, H., Prandina, M., Mottershead, J. E., Swift, A., Da Ronch, A., and Woodgate, M. A., "Transonic aeroelastic simulation for instability searches and uncertainty analysis," *Progress in Aerospace Sciences*, Vol. 47, No. 5, 2011, pp. 392–423.

[9]Badcock, K. J. and Woodgate, M. A., "Bifurcation prediction of large–order aeroelastic models," *AIAA Journal*, Vol. 48, No. 6, 2010, pp. 1037–1046.

[10]Timme, S. and Badcock, K. J., "Transonic aeroelastic instability searches using sampling and aerodynamic model hierarchy," *AIAA Journal*, Vol. 49, No. 6, 2011, pp. 1191–1201.

[11]Timme, S., Marques, S., and Badcock, K. J., "Transonic aeroelastic stability analysis using a kriging–based Schur complement formulation," *AIAA Journal*, Vol. 49, No. 6, 2011, pp. 1202–1213.

[12]Meerbergen, K. and Spence, A., "Inverse iteration for purely imaginary eigenvalues with application to the detection of Hopf bifurcations in large–scale problems," *SIAM. J. Matrix Anal. & Appl.*, Vol. 31, No. 4, 2010, pp. 1982–1999.

[13]Elman, H. C., Meerbergen, K., Spence, A., and Wu, M., "Lyapunov inverse iteration for identifying Hopf bifurcations in models of incompressible flow," Tech. Rep. TR–4975, TR–2011–04, University of Maryland, 2011, to appear in SIAM. J. Sci. Comp.

[14]Saad, Y., "Numerical solution of large Lyapunov equations," *in M. A. Kaashoek, J. H. van Schuppen, and A. C. Ran (Eds.), Signal Processing, Scattering and Operator Theory, and Numerical Methods, Proc. MTNS-89*, Birkhauser, Boston, MA, 1990, pp. 503–511.

[15]Robbe, M., Sadkane, M., and Spence, A., "Inexact inverse subspace iteration with preconditioning applied to non–Hermitian eigenvalue problems," *SIAM. J. Matrix Anal. & Appl.*, Vol. 31, No. 1, 2009, pp. 92–112.

[16]Badcock, K. J., Richards, B. E., and Woodgate, M. A., "Elements of computational fluid dynamics on block structured grids using implicit solvers," *Progress in Aerospace Sciences*, Vol. 36, 2000, pp. 351–392.

[17]Fung, Y. C., *An introduction to the theory of aeroelasticity*, John Wiley & Sons, Inc., New York, NY, 1955.

[18]Löhner, R., Sacco, C., Onate, E., and Idelsohn, S., "A finite point method for compressible flow," *Int. J. Numer. Meth. Engng*, Vol. 53, 2002, pp. 1765–1779.

[19]Kennett, D. J., Timme, S., Angulo, J., and Badcock, K. J., "An implicit semi–meshless scheme with stencil selection for anisotropic point distributions," *AIAA Paper 2011–3234*, 2011.

[20]Badcock, K. J., Khodaparast, H. H., Timme, S., and Mottershead, J. E., "Calculating the influence of structural uncertainty on aeroelastic limit cycle response," *AIAA Paper 2011–1741*, 2011.

[21]Beran, P. S., Khot, N. S., Eastep, F. E., Snyder, R. D., and Zweber, J. V., "Numerical analysis of store–induced limit–cycle oscillation," *Journal of Aircraft*, Vol. 41, No. 6, 2004, pp. 1315–1326.

[22]Crouch, J. D., Garbaruk, A., and Magidov, D., "Predicting the onset of flow unsteadiness based on global instability," *Journal of Computational Physics*, Vol. 224, No. 2, 2007, pp. 924–940.

[23]Williamson, C. J. K., "Vortex dynamics in the cylinder wake," *Annu. Rev. Fluid Mech.*, Vol. 28, 1996, pp. 477–539.

[24]Hammache, M. and Gharib, M., "An experimental study of the parallel and oblique vortex shedding from circular cylinders," *J. Fluid Mech.*, Vol. 232, 1991, pp. 567–590.